Exploring Nanomechanical Behavior of Silicon Nanowires: AFM Bending Versus Nanoindentation

Yong-Jae Kim, Kwangsoo Son, In-Chul Choi, In-Suk Choi, Won Il Park, and Jae-il Jang**

Despite many efforts to advance the understanding of nanowire mechanics, a precise characterization of the mechanical behavior and properties of nanowires is still far from standardization. The primary objective of this work is to suggest the most appropriate testing method for accurately determining the mechanical performance of silicon nanowires. To accomplish this goal, the mechanical properties of silicon nanowires with a radius between 15 and 70 nm (this may be the widest range ever reported in this research field) are systematically explored by performing the two most popular nanomechanical tests, atomic force microscopy (AFM) bending and nanoindentation, on the basis of different analytical models and testing conditions. A variety of nanomechanical experiments lead to the suggestion that AFM bending based on the line tension model is the most appropriate and reliable testing method for mechanical characterization of silicon nanowires. This recommendation is also guided by systematic investigations of the testing environments through finite element simulations. Results are then discussed in terms of the size-dependency of the mechanical properties; in the examined range of nanowire radius, the elastic modulus is about 185 GPa without showing significant size dependency, whereas the nanowire strength dramatically increases from 2 to 10 GPa as the radius is reduced.

1. Introduction

One-dimensional (1D) nanomaterials including nanowires, nanorods, and nanotubes have attracted considerable interest from the interdisciplinary areas in science and engineering because of their unique and excellent mechanical, electrical, and optical properties. In particular, silicon (Si) nanowires have been considered to be one of the most technologically important building blocks for emerging bottom-up nanotechnology and have been used as the active components in a broad range of electronic devices such as field effect transistors,[1,2] chemical and biological sensors,[3] photodetectors,[4] and solar cells.[5] Since a fundamental knowledge of nanowire mechanics is essential for designing, manufacturing, and reliably operating nanowire-based nanodevices, the precise measurement of the mechanical behavior and properties in nanowires has been gathering not only scientific but also practical interest. In particular, as significant progress has been made toward flexible and stretchable nanowire electronics, the understanding and control of mechanical behavior at the nanoscale have become more important.

A variety of experimental approaches have been developed including a lateral or normal bending test using atomic force microscopy (AFM),[6–10] an instrumented nanoindentation test,[11–14] a resonant frequency (or electric-field-induced oscillation) test,[15,16] a buckling test (especially for so-called nanoforests),[17] and in situ bending and tensile testing.[18,19] Among these, AFM-based bending[6–8] and nanoindentation[11–13] are the most popularly adopted testing methods for measuring both elastic and plastic properties[20] due to their advantages of easy preparation, convenient manipulation, and high spatial resolution. However, even these two methods are still far from standardization and the experimental results have shown large discrepancies. For example, although it has often been proposed[6–8] that appropriate analysis of AFM bending data can lead to the full spectrum of mechanical properties from elastic deformation to failure, an important question, "Which analytical model would provide more accurate values?" remains unresolved. Several issues also exist for nanoindentation of nanowires, e.g., the influences of the substrate (in a similar manner to that adopted in previous thin film studies),[21] the rounded surface of the nanowires,[22] and the indenter tip bluntness.[21] Sometimes the nanoindentation experiments are conducted with AFM[14] instead of a commercial indentation equipment, but the inherent shortcomings, such as the difficulty of perpendicular contact and the deflection of the cantilever, make it difficult to yield precise results.

With these in mind, the primary objective of this work was set to suggest the most appropriate and reliable testing method for precisely determining the mechanical properties of Si nanowires. To accomplish this goal, we have estimated the

Y.-J. Kim, K. Son, I.-C. Choi, Prof. W. I. Park, Prof. J.-i. Jang
Division of Materials Science and Engineering
Hanyang University
Seoul 133–791, Korea
E-mail: jijang@hanyang.ac.kr; wipark@hanyang.ac.kr
Dr. I.-S. Choi
High Temperature Energy Center
Korea Institute of Science and Technology
Seoul 136–791, Korea

DOI: 10.1002/adfm.201001471

elastic modulus and yield (or failure) strength of <111>-oriented Si nanowires grown by vapor-liquid-solid (VLS) method via two most popular nanomechanical tests, AFM bending and nanoindentation, on the basis of different analytical models and testing conditions. The results from different analyses were systematically investigated and then directly compared to provide a fundamental guideline for legitimate mechanical measurement. Furthermore, to our best knowledge, these experimental data cover the widest range of nanowire radius (15–70 nm) ever reported before in this research field, and thus it is hoped that the evaluated nanowire strength for a wider range would be valuable for better understanding of nanowire mechanics.

2. Results and Discussion

2.1. AFM Bending

Figure 1a shows a representative lateral force–displacement (*F*–*d*) curve obtained from AFM bending experiments (for details, see Experimental Section). Since the output signal of AFM bending was voltage *V* (i.e., photodiode signal) as a function of displacement, *d*, as shown in the inset graph of Figure 1a, it was converted to the absolute value of lateral force, *F*, using the following equation:[23]

$$F = \left(\frac{E_{\text{can}} w t^3}{6 l^2 a}\right)\left(\frac{1}{S_{\text{ver}}}\right) V \tag{1}$$

where E_{can}, w, t, and l are the elastic modulus, width, thickness, and length of the cantilever, respectively; a is the AFM tip height; and S_{ver} is the vertical sensitivity, which means the slope of *V*–*d* curves during forcing on a hard surface. In the figure, a sharp drop in force corresponds to the brittle failure of the Si nanowire, which was confirmed by examining the AFM image taken immediately after the test (inset of Figure 1a).

Since two types of forces, bending and line tension (along the axial direction), can evolve during an AFM bending test of nanowire, there are three possible analytical models applicable to the extraction of elastic modulus and yield strength from AFM *F*–*d* curve: The first is the bending-only model (without considering line tension) based on the conventional elastic beam-bending theory, where *F*–*d* relationship for an elastic deformation and yield strength σ_y can be given by[6]

$$F = \frac{48\pi r^4 E}{L^3} \cdot d \tag{2}$$

and

$$\sigma_y = \frac{F_y L}{2\pi r^3} \tag{3}$$

where E, r, and L are the elastic modulus, radius, and span length of nanowire, respectively, and F_y is the load at the onset of failure. The second is the line-tension-only model in which an axial tensile force along the nanowire is predominant and thus bending force is not considered. The line tension analysis gives equations of *F*–*d* relation and σ_y as:[7]

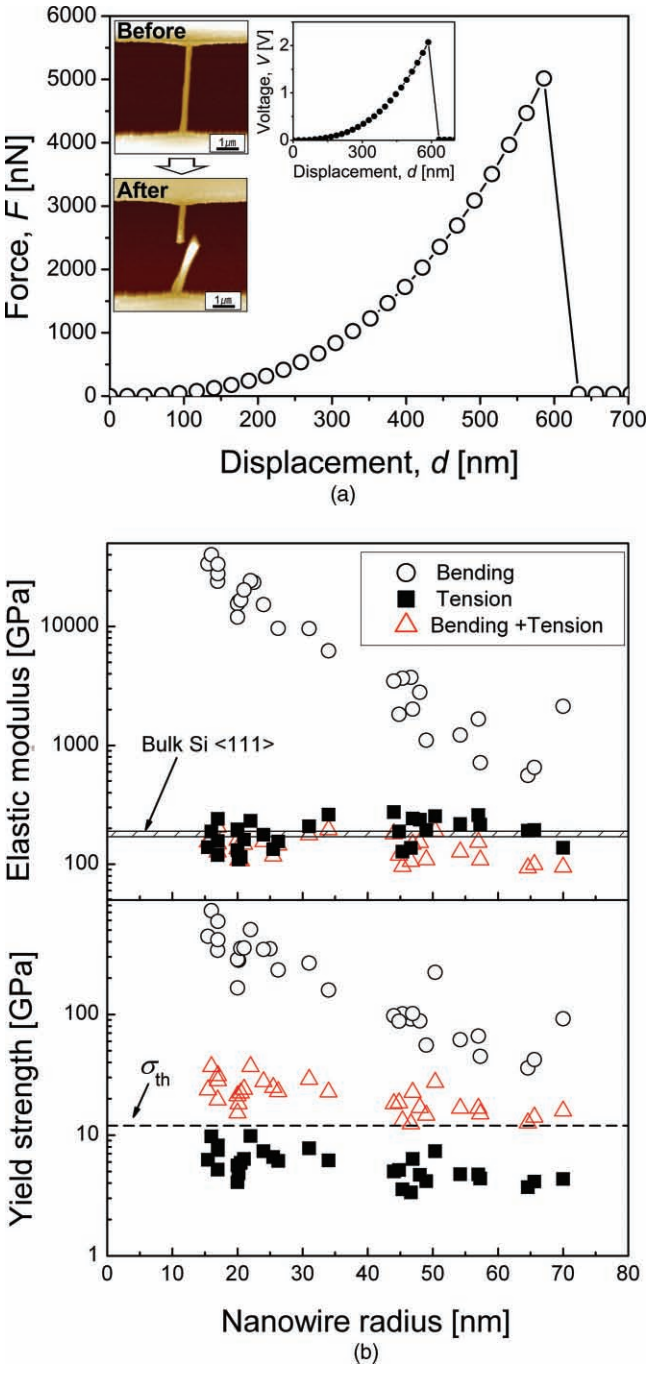

Figure 1. Results from AFM bending experiments. a) Representative *F*–*d* curve from an AFM bending test. The inset images are the AFM images taken before and after bending test and the *V*–*d* curve before conversion to the *F*–*d* curve. b) Summary of elastic modulus and yield strength extracted from AFM bending.

$$F = \frac{8\pi r^2 E}{L^3} \cdot d^3 \tag{4}$$

and

$$\sigma_y = \frac{F_y L}{4\pi r^2 d_y} \tag{5}$$

where d_y is the displacement at failure. The last is the combined bending-tension model. This model was derived to account for both bending and line tension together, and the equations are given as in the form of the bending-only model with correction function $f(\alpha)$ and $g(\alpha)$:[8]

$$F = \frac{48\pi r^4 E}{L^3} \cdot d \cdot f(\alpha) \tag{6}$$

and

$$\sigma_y = \frac{F_y L}{2\pi r^3} \cdot g(\alpha). \tag{7}$$

The function $f(\alpha)$ and $g(\alpha)$ are defined as

$$f(\alpha) = \frac{\alpha}{48 - \frac{192 \cdot \tanh\left(\sqrt{\alpha}/4\right)}{\sqrt{\alpha}}} \tag{8}$$

and

$$g(\alpha) = \frac{4}{\sqrt{\alpha}} \cdot \tanh\left(\frac{\sqrt{\alpha}}{4}\right) + \sqrt{\frac{2 + \cosh\left(\sqrt{\alpha}/2\right) - 6 \cdot \sinh\left(\sqrt{\alpha}/2\right)/\sqrt{\alpha}}{\alpha \cdot \cosh^2\left(\sqrt{\alpha}/4\right)}} \tag{9}$$

where α is related to nanowire radius and displacement by

$$\alpha = \frac{6\varepsilon(140 + \varepsilon)}{350 + 3\varepsilon} \tag{10}$$

and

$$\varepsilon = \left(\frac{2d}{r}\right)^2. \tag{11}$$

Collectively, the relation between F and d is linear for the bending-only model and non-linear for the others. As noticed in Equation 3, 5, and 7, the yield strength based on any model could be easily calculated by putting F and d at the point of failure (i.e., F_y and d_y) into the equations.[24] However, to extract the elastic modulus, different methods were applied: in the bending-only and tension-only approaches, the elastic modulus was extracted by properly fitting the loading curve (in Figure 1a) following the theoretical F–d relation (Equation 2,4), whereas in the case of the combined bending-tension model, the elastic modulus was calculated by putting F and d at failure into Equation 7 because the correction function in Equation 6 was too complex to be used for fitting the experimental data. It should be noted that for a brittle material such as bulk Si under external stresses, the end of elastic deformation (i.e., yielding) is often more closely related to fracture (controlled by crack-like flaws) than plastic deformation (activated by crystalline defects, i.e., dislocations). However, the detailed mechanism of the nanoscale yielding has not been fully understood yet. Thus, in this study, the strength at the end of elastic deformation is just called "yield strength," which encompasses all feasible mechanisms for finishing the elastic deformation. This is acceptable because almost no difference between yield strength and failure strength is generally observed in the uniaxial tests of brittle materials exhibiting a small-scale yielding.

Figure 1b summarizes the elastic modulus, E, and yield strength, σ_y, obtained from each model as a function of nanowire radius. In the plot of the logarithm of E and σ_y against the radius, the bending-only model yielded an inversely linear relation of the properties against the radius for a wide range (i.e., 600–40000 GPa for E and 35–700 GPa for σ_y). For the tension-only model, the E was 186.1 GPa ± 47.7 GPa and was almost independent of radius over the investigated range, while σ_y increased from 2 to 10 GPa as the nanowires became smaller. In the case of the combined bending-tension model, E was 141.9 GPa ± 33.3 GPa with no size dependency and σ_y increased from 12 to 37 GPa with reducing the radius.

From these experimental results, one may find a clue as to which model is the most appropriate for estimating the properties of nanowires (or at least the Si nanowires examined here). First of all, the results from the bending-only model may not be reasonable; the E values are much higher than those reported in the literature (170–190 GPa[25,26] as marked in Figure 1b; some indentation results provide higher values[27–29]) and the σ_y values are higher than the theoretical yield strength ($\sigma_{th} = 2\tau_{th} \approx G/5 \approx 12$ GPa where $G \approx 60$ GPa,[30,31] marked in the lower panel of Figure 1b) and even than the theoretical cohesive strength ($\sigma_{th,coh} \approx E/10 \approx 18$ GPa). One may easily imagine that this unlikely result came from a linear F–d relation in Equation 2, which cannot explain the non-linear shape of the experimental curve. Next, in the case of the combined bending-tension model, the E values are within a reasonable range though they are slightly smaller than those in the literature. However, the fact that the σ_y values are higher than σ_{th} makes this model appear to be inappropriate as well. Finally, the tension-only model seems to provide the most reasonable results for both the E values, which are very close to the literature values, and the σ_y values, which become more comparable to the theoretical values as nanowire radius is reduced. Therefore, we could reach the conclusion that the adoption of the tension-only model is the most valid here.

To support this conclusion, a series of 3D finite element simulations were conducted (see **Figure 2**a, which shows a representative example of elastic strain distribution during AFM bending). In the simulations, the nanowire (with the same size as that of the tested nanowire) was loaded until it failed. As representatively shown in Figure 2b, the F–d curve extracted from simulations is in good agreement with that of experiment. It is important to note that the F–d relation is dependent on the ratio of the maximum displacement to the nanowire radius (d_{max}/r). The inset images of Figure 2b show examples of the simulation results together with the theoretically fitted values; the dashed line and the solid curve are based on the bending-only (Equation 2) and the tension-only model (Equation 4) respectively. As shown in the figure, when d_{max}/r is relatively small (see the example of $d_{max}/r = 1$), F increases almost linearly with d. However, as d_{max}/r increases, the F–d relation is no longer linear (see the inset for $d_{max}/r = 5$, where the F–d curve is between the line from the bending model and the curve from the tension model). For very high d_{max}/r (the experimental data in Figure 2b), F could be successfully described as a linear function of d^3, implying that Equation 4 of the

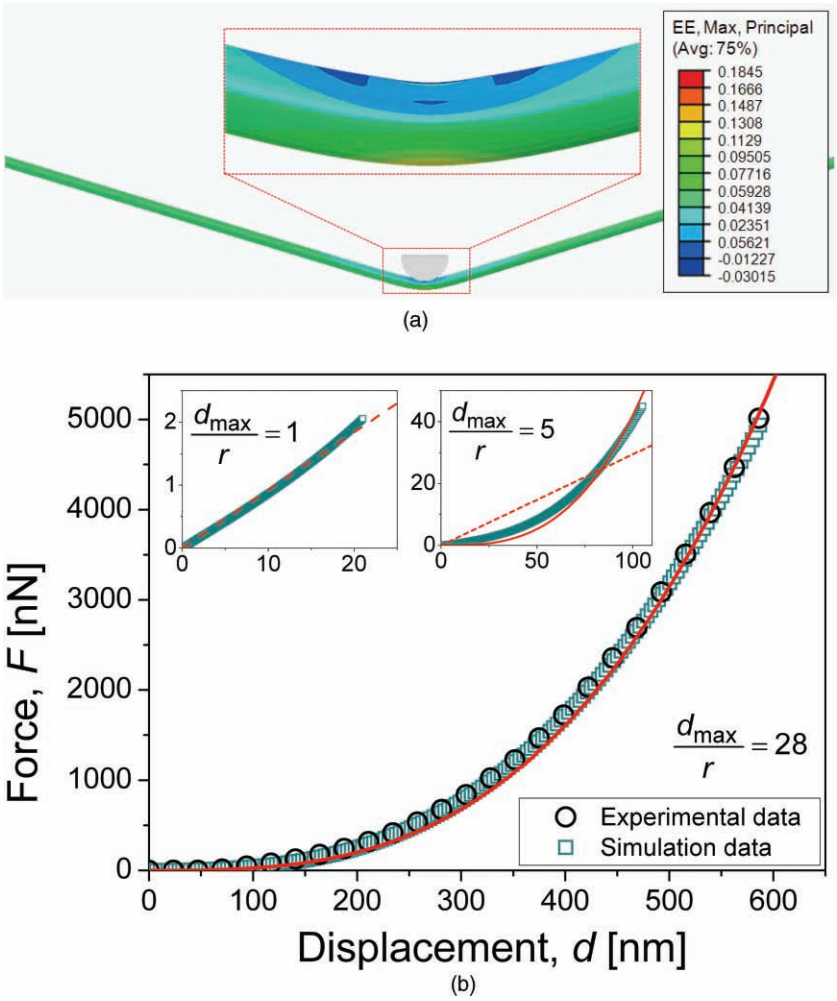

Figure 2. Representative examples of the results from 3D finite element simulations. a) Elastic strain distribution during AFM bending ($d_{max}/r = 28$). b) *F–d* curves from bending experiments and finite element simulations ($d_{max}/r = 28$). The inset images are *F–d* curves for the cases of $d_{max}/r = 1$ and $d_{max}/r = 5$, in which *F–d* simulation data are fitted with the bending-only model (dashed line) and the tension-only model (solid curve).

tension-only model is applicable. Note that at the displacement of failure in Figure 2b ($d_{max} \approx 600$ nm), the theoretical bending force is negligibly small (less than 1% of theoretical tension force). Therefore, one may imagine that as the d_{max}/r ratio increases, the proper analytical model would change from the bending-only model to the combined bending-tension model and then finally to the tension-only model (for very high values of d_{max}/r). Based on the experimental and simulated results, it is possible to propose a way to select an appropriate analytical model for AFM bending tests of Si nanowires. The bending-only model (Equation 2,3) can be successfully applied when the d_{max}/r is smaller than unity and/or the *F–d* relation is linear. For a nonlinear *F–d* relation, the combined bending-tension model can be adopted for $d_{max}/r \approx 1$–20 and the tension-only model for $d_{max}/r > 20$, the range in which all of our AFM bending tests lie. It is noteworthy that our suggestion is based on Si nanowire bending with a span length of 4 μm and thus the detailed boundary values of d_{max}/r between each model can be varied when different span lengths and materials are applied.

2.2. Nanoindentation

Now, we turn our attention into the nanoindentation experiments (for details, see Experimental Section). **Figure 3**a shows load–displacement (*P–h*) curves obtained from nanoindentation with a typical Berkovich indenter and a sharper cube-corner indenter having centerline-to-face angles of 65.3° and 35.3°, respectively. At a given load, the sharper cube-corner indenter produced much higher displacement than the Berkovich indenter. Inset images show a representative example of the indentation impression made in the center of the nanowire. The elastic modulus, *E*, and the hardness, *H*, were calculated according to the commonly used Oliver–Pharr method.[32] Tabor's empirical equation,[33] $\sigma_y = CH$, with a constraint factor *C* of about 2.5[34] was used to estimate σ_y from *H*. In Figure 3b, the *E* and σ_y from nanoindentation are plotted against the nanowire radius. No obvious trend can be found in the changes in *E* and σ_y with the radius. For Berkovich indentation, average values of *E* and σ_y were 37.9 GPa ± 13.3 GPa and 0.8 GPa ± 0.4 GPa, respectively, which are two or three times smaller than the values measured with the cube-corner tip (*E* = 59.5 GPa ± 13.3 GPa and σ_y = 2.3 GPa ± 0.9 GPa).

One of the possible reasons for the much higher hardness of the cube-corner indentation is the effect of the rounded surface of the nanowire[22] on the predicted contact area. **Figure 4**a is a schematic illustration presenting the influences of surface roundness and tip geometry on the contact radius, r_c. The left-hand side of the figure is for the Berkovich indentation, while the other side exhibits cube-corner indentation. Since the Oliver–Pharr method fundamentally requires a flat sample surface, a significant error can be made if one applies this method to analyze the results of the indentation on a rounded surface; that is, as shown in Figure 4a, if one calculates the contact area *A* of the rounded sample according to the Oliver–Pharr method (in which the surface is assumed to be flat), the calculated *A* will be overestimated and thus the indentation hardness *H* (= *P*/*A*) and the elastic modulus *E* (which is proportional to $A^{-0.5}$) can be overestimated. From the figure, it is also possible to expect that the use of a sharper indenter may reduce the difference between the calculated and real contact area. To further support this hypothesis, 2D finite element analysis of Si was performed for both a rounded surface nanowire and a flat surface film. To simplify the simulations, the substrate and the conical indenters (having half-included angles of 70.3° and 42.3°, which are equivalent to a Berkovich and cube-corner

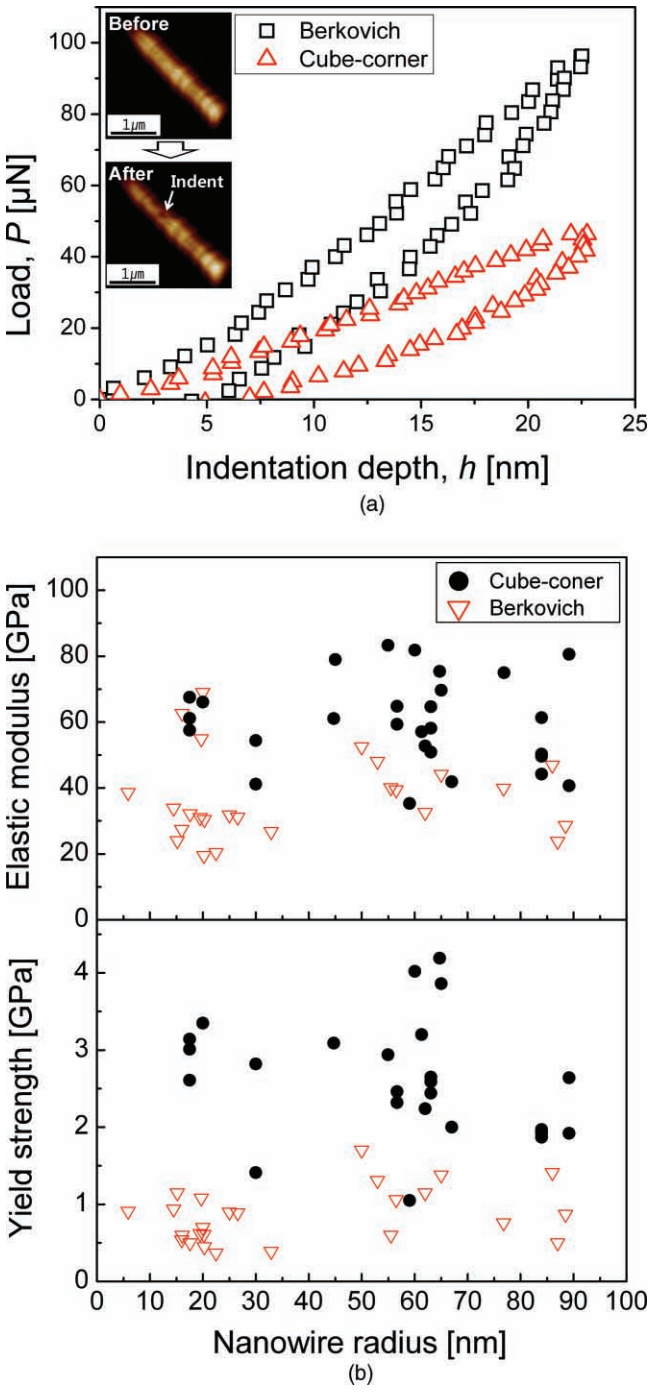

Figure 3. Results from nanoindentation experiments. a) Representative *P–h* curves from nanoindentation with Berkovich and cube-corner tips. The inset images are the representative AFM images taken before and after the experiment. b) Summary of elastic modulus and yield strength obtained from nanoindentation with the two tips.

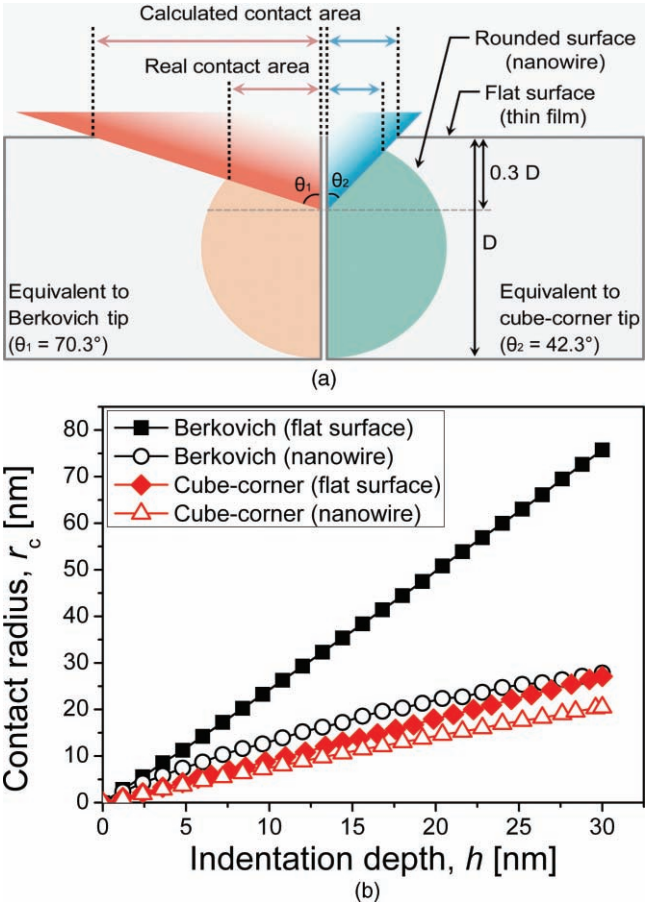

Figure 4. The rounded surface effect on the contact area. a) Schematic illustrations for comparison between Berkovich (left-hand side) and cube-corner indentation (right-hand side) on both rounded and flat surface. b) Contact radius estimated by finite element simulations.

indenter, respectively) were assumed to be rigid, and the maximum indentation depth was fixed as 30% of their diameter or thickness. The results are shown in Figure 4b where the values of the contact radius r_c are plotted against indentation depth h. It is seen in the figure that, regardless of the tip geometry, the r_c for flat surface is larger than that for the rounded surface. Additionally, the cube-corner indentation produces a much smaller difference in the r_c value between the flat and rounded surface than the Berkovich indentation. However, even in the cube-corner indentation, the r_c for a flat surface at h_{max} = 30 nm is still 1.3 times larger than that for rounded surface so that the underestimation of modulus and hardness is inevitable. Besides the overestimation of the contact area, another possible reason for the underestimated hardness and modulus is the sample boundary effect in a way similar to that suggested by Lian et al.[35] for the indentations on the nano- and micropillars; the deformation in a sample with finite boundaries is less constrained by surrounding materials (unlike in a semi-infinite half plane) and, thus, may result in a decrease in both stiffness and hardness. Collectively, it seems difficult to realize the precise mechanical characterization of nanowire by nanoindentation based on the Oliver–Pharr method.

2.3. Comparison and Size Effect

The main question we posed earlier ("Which technique is the most appropriate and reliable for the precise mechanical

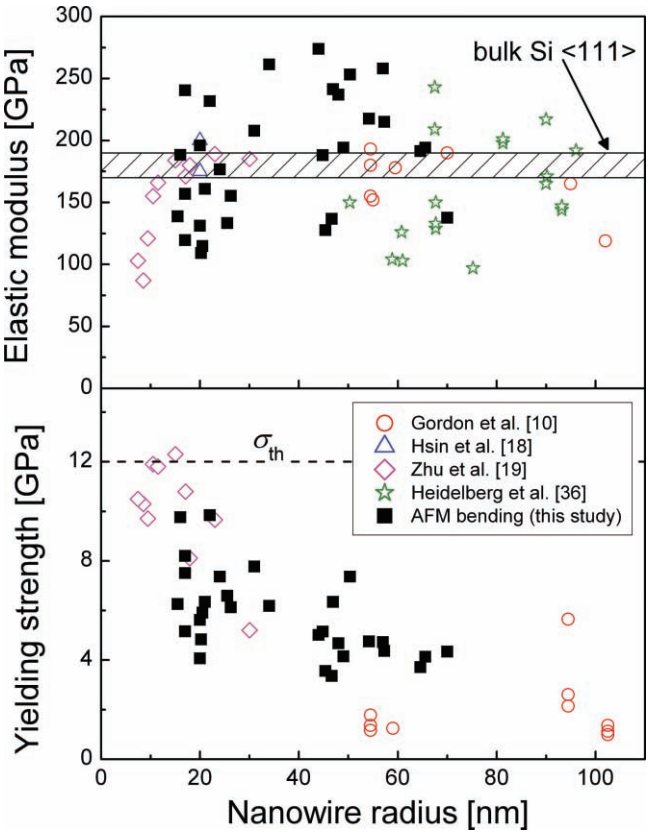

Figure 5. Variation in the elastic modulus and yield strength of Si nanowires (obtained in present and previous studies[10,18,19,36]) as a function of nanowire radius.

property measurement of Si nanowire?") may be addressed by simply comparing the values from AFM bending (the tension-only model data in Figure 1b) and those from nanoindentation (the cube-corner indentation data in Figure 3b); that is, AFM bending with the tension-only analysis may be better than nanoindentation. Although the cube-corner tip produced more reasonable values than the Berkovich tip, it is still not free from the rounded-surface effect and sample boundary effect. In **Figure 5**, the elastic modulus and yield strength from AFM bending based on the tension-only model are replotted with the values reported in the previous studies.[10,18,19,36] There is a good agreement between present and previous data. Note that only the data showing a good fit of the F–d^3 relation in Equation 4 (correction factor $R^2 > 0.75$) are presented in the figure.

In Figure 5, as the nanowire radius was reduced from 70 to 15 nm, the elastic modulus was not significantly changed and remained almost constant at about 185 GPa, whereas the yield strength increased from 2 to 10 GPa. There have been many studies devoted to analyzing the size dependency of the elastic modulus and yield strength of nanowires. First, the effect of nanowire size on the elastic modulus is somewhat controversial and strongly dependent on the nanowire material; for example, Stan et al.[14] and Jing et al.[9] reported that the E of ZnO and metallic (silver) nanowires increased with decreasing radius (which has been often explained by energy pinning theory based on Goldschmidt–Pauling's rule of bond contraction),[37,38] while Zhu et al.[19] observed an opposite trend, i.e., elastic softening, for Si nanowires (see Figure 5), that is, E decreased with reduced radius. The most likely mechanisms for the size-dependent elastic modulus of Si nanowires are the surface reconstruction[39] and the existence of surface oxide/amorphous layer.[10] Surface reconstruction can be caused by broken bonds in surface atoms in order to lower the surface energy. Since Si nanowires are often covered with an amorphous silicon oxide layer in which atoms are randomly distributed and the surface energy is minimized, this reconstruction effect is thought to be a minor factor in the softening effect. Also, considering that the E of amorphous silicon oxide was reported to be about 75 GPa[40] and is much smaller than that of silicon, the elastic softening with reduced size can be caused by the surface oxide layer despite its thickness of less than 5 nm. However, in our experiments, the trend of elastic softening with reduced radius is not manifested (see Figure 5). This disagreement between present and previous work[19] may arise from the difference in the examined range of the nanowire radius; the previous simulation[41,42] and experimental work[19] reported that the elastic softening of Si nanowires is obvious when the radius is smaller than 15 nm, but the radius range investigated here is 15–70 nm, where the modulus is supposed to be constant.

In contrast to the elastic modulus, the genearlly accepted "the smaller, the stronger" rule is clearly observed in the plot of the yield strength versus nanowire radius in Figure 5. For <111>-oriented Si nanowires, such trend agrees with the previous results,[10,19] as seen in the figure. The different trends of size effect for elastic modulus and yield strength may conceivably come from the fact that the latter is much more seriously affected by the defects in nanowires. As mentioned earlier, the end of elastic deformation (i.e., yielding) in Si is often more closely related with fracture than deformation and the fracture may occur, even on the nanoscale, by the sudden and catastrophic growth of cracks that initiate at the flaws or crystalline defects. Since Si nanowires grown by VLS-method are well known to have an almost flaw-free internal structure, cracking can be assumed to initiate at the surface flaws. For nanowires with smaller size, there is less possibility of surface flaws, leading to an increase in the yield strength. In particular, there seems to be a transition in size-dependency around 30 nm, where the decreasing rate of the nanowire strength becomes abruptly changed. While this might conceivably be associated with a drastic change in surface flaw density,[19] further studies to clarify possible mechanisms are desirable.

On the other hand, we showed in the previous section that the cube-corner indentation is more accurate than the Berkovich indentation. Since the indentation depth was set to be 30% of nanowire diameter, relative comparison of the plasticity onset for different sizes of nanowires was acceptable in a qualitative manner, although we could not extract the absolute values of the strength even with a cube-corner indenter. As shown in Figure 3, the yield strength measured with the cube-corner indenter increases with decreasing radius, which also confirms the size-dependency in yield strength.

Before closing, it is constructive to note again that, if we focus on the size below 100 nm, to our best knowledge, our experimental data for the σ_y versus r relations may cover the widest range of nanowire radius ever reported before (see

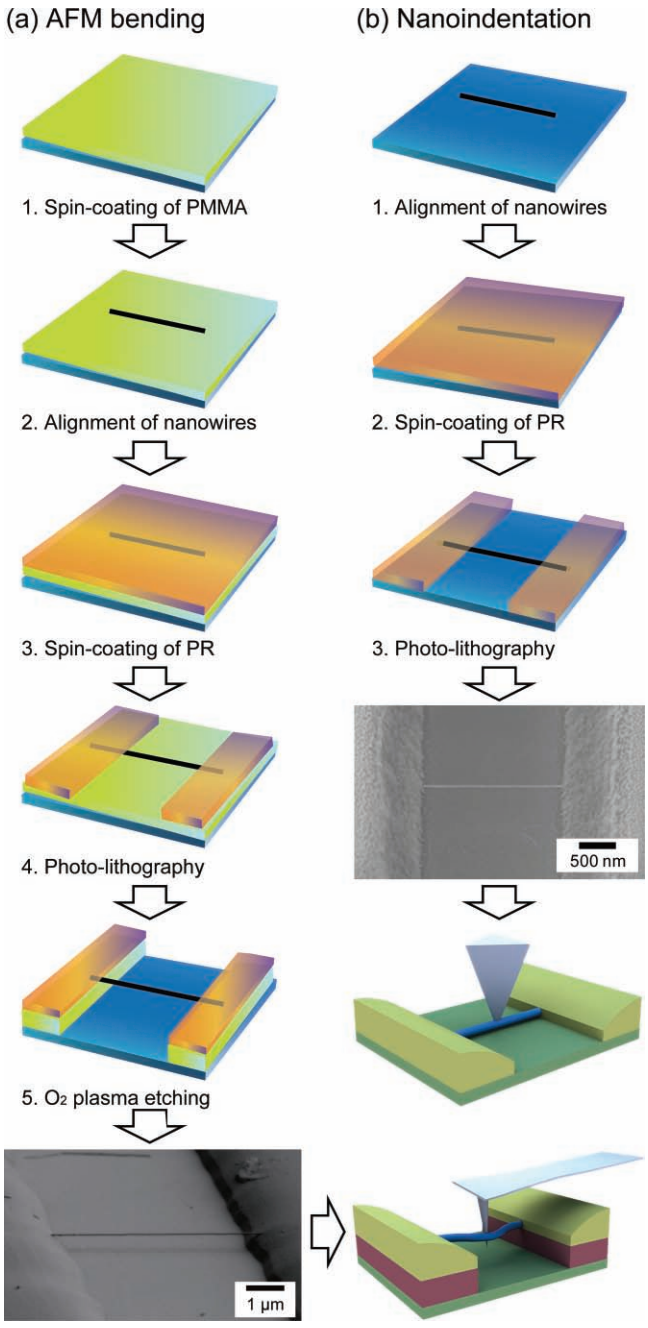

Figure 6. Schematic diagrams showing the preparation procedures for the testing structures (including SEM images of fabricated structures). a) AFM bending and b) nanoindentation.

Figure 5). Therefore, now the size-dependency of the yield strength becomes much clearer for a wider range of radii, which might contribute to a further step towards a complete understanding of nanowire mechanics.

3. Conclusions

A variety of nanomechanical tests have been systematically performed to accurately determine the elastic modulus and yield strength of VLS-grown <111> Si nanowires with radii between 15 and 70 nm (which may be the widest range in this research field). Direct comparison of the experimental results revealed that the AFM bending based on the line tension model provided the most accurate mechanical properties of Si nanowires. The experimental guideline of the AFM bending test was also provided by a series of systematic finite element simulations. Then, the size-dependency of the mechanical properties was investigated for a wide range of nanowire radii from 15 to 70 nm. The estimated elastic modulus of Si nanowires was about 185 GPa and does not significantly change with the size of nanowire, whereas the yield strength showed a strong size effect and increased from 2 to 10 GPa with reduced radius.

It is hoped that these results and suggestions will be valuable for establishing reliable ways to estimate mechanical performance of semiconducting nanowires. Nevertheless, for providing more practical information in the field of the nanowire-based optoelectric device fabrication, there are some remaining questions that are desirable to be addressed in future studies, for example, "How can the doping (which is required to be precisely made during the fabrication) affect the mechanical properties of silicon nanowires?" Note that the effect is still very controversial even for bulk Si samples, i.e., some[43,44] reported the properties were enhanced by doping, but others[45,46] showed the doping could deteriorate the properties. More importantly, many more III–IV group nanowires must be tested and analyzed to evaluate critically the applicability of the results.

4. Experimental Section

The examined Si nanowires were synthesized in a horizontal tube furnace equipped with a 1.5 in. diameter quartz tube via a Au nanocluster-catalyzed VLS method.[47] Using solution-deposited Au colloids with diameters in the range of 20–100 nm, single-crystal Si nanowires with radii between 15 and 90 nm and lengths of more than 10 μm were obtained.

Figure 6 schematically illustrates the fabrication procedures for two testing structures with double clamped Si nanowire arrays: (i) suspended nanowires for AFM bending and (ii) nanowires laid on the substrate surface for nanoindentation. For the testing structure of AFM bending (Figure 6a), a 300-nm-thick poly(methyl methacrylate) (PMMA) layer was initially spin-coated on the SiO_2/Si substrate and baked at 120 °C for 2 min. Horizontally aligned Si nanowire arrays were then deposited on the PMMA layer by the contact print method,[48] followed by spin-coating of a photoresist (PR) AZ1512 layer on the aligned wires. The PR line patterns were defined by the conventional photolithography process. Soft- and hard-baking (95 °C for 1 min and 120 °C for 2 min, respectively) were performed before and after the lithography process. Subsequently, O_2 plasma etching was conducted using the remaining PR as an etching mask, in order to etch the exposed PMMA and thus to fabricate appropriate trenches. In final structure, both ends of the nanowire were clamped by the PMMA and PR layers, which were sufficiently cured. The depth of the trench was about 200–300 nm, which is almost same as the thickness of PMMA. The width of the trench was about 4 μm and could be controlled by varying the lithograph mask size or O_2 plasma etching time. On the other hand, the process for a testing structure for nanoindentation (Figure 6b) was similar to that of AFM bending, except for the initial PMMA coating; the sequences consisted of arraying nanowires on the substrate, spin-coating PR, a photolithography process, and O_2 plasma etching. Representative examples of the final structures for both AFM bending and nanoindentation are shown in the scanning electron microscopy (SEM) images in Figure 6.

Optical microscopy using dark-field mode (BX51, Olympus, UK) and field-emission SEM (FE-SEM, S-4800, Hitach, Japan) were used for selecting well-aligned nanowires and characterizing the geometry of both nanowires and the AFM cantilever. AFM bending tests were carried out using an XE-100 (Park Systems, Suwon, Korea) with the non-contact mode cantilever having a spring constant of 40 N m^{-1}, while nanoindentation was performed by using Triboindenter (Hysitron Inc., Minneapolis, MN) with two different three-sided pyramidal diamond indenters having different centerline-to-face angles, ψ; a typically used Berkovich ($\psi = 65.3°$) and sharper cube-corner tip ($\psi = 35.3°$). After a series of nanoindentations on fused quartz, the area function of the indenter tip was calibrated in the range of contact depth we were interested in. Thermal drift correction was made before each test. To avoid serious substrate effects, the maximum indentation depth was kept to less than 30% of the nanowire diameter.[11] In addition to the experimental analysis, a series of finite element simulations was also performed with ABAQUS (HKS Inc., Pawtucket, RI) software. The eight-node 3D mesh comprised of 38 080 linear elements was used for the bending simulation, while the four-node axi-symmetric mesh comprised of 10 000 (and 4 821) linear elements was used for the simulation of the indentation on the flat (and rounded) surface.

Acknowledgements

This work was supported by the Mid-Career Researcher Program through NRF grant funded by the MEST (No. R01–2008-000–20778-0).

Received: July 20, 2010
Revised: September 14, 2010
Published online: November 15, 2010

[1] R. Beckman, E. Johnston-Halperin, Y. Luo, J. E. Green, J. R. Heath, *Science* **2005**, *310*, 465.
[2] J. Goldberger, A. I. Hochbaum, R. Fan, P. Yang, *Nano Lett.* **2006**, *6*, 973.
[3] F. Patolsky, C. M. Lieber, *Mater. Today* **2005**, *8*, 20.
[4] O. Hayden, R. Agarwal, C. M. Lieber, *Nat. Mater.* **2006**, *5*, 352.
[5] M. D. Kelzenberg, D. B. Turner-Evans, B. M. Kayes, M. A. Filler, M. C. Putnam, N. S. Lewis, H. A. Atwater, *Nano Lett.* **2008**, *8*, 710.
[6] B. Wu, A. Heidelberg, J. J. Boland, *Nat. Mater.* **2005**, *4*, 525.
[7] D. Almecija, D. Blond, J. E. Sader, J. N. Coleman, J. J. Boland, *Carbon* **2009**, *47*, 2253.
[8] B. Wen, J. E. Sader, J. J. Boland, *Phys. Rev. Lett.* **2008**, *101*, 175502.
[9] G. Y. Jing, H. L. Duan, X. M. Sun, Z. S. Zhang, J. Xu, Y. D. Li, J. X. Wang, D. P. Yu, *Phys. Rev. B* **2006**, *73*, 235409.
[10] M. J. Gordon, T. Baron, F. Dhalluin, P. Gentile, P. Ferret, *Nano Lett.* **2009**, *9*, 525.
[11] X. Li, H. Gao, C. J. Murphy, K. K. Caswell, *Nano Lett.* **2003**, *3*, 1495.
[12] G. Feng, W. D. Nix, Y. Yoon, C. J. Lee, *J. Appl. Phys.* **2006**, *99*, 074304
[13] X. Tao, X. Li, *Nano Lett.* **2008**, *8*, 505.
[14] G. Stan, C. V. Ciobanu, P. M. Pathangal, R. F. Cook, *Nano Lett.* **2007**, *7*, 3691.
[15] Z. L. Wang, R. P. Gao, P. Poncharal, W. A. de Heer, Z. R. Dai, Z. W. Pan, *Mater. Sci. Eng., C* **2001**, *16*, 3.
[16] C. Q. Chen, Y. Shi, Y. S. Zhang, J. Zhu, Y. J. Yan, *Phys. Rev. Lett.* **2006**, *96*, 075505.
[17] R. Dou, B. Derby, *Scr. Mater.* **2008**, *59*, 151.
[18] C. L. Hsin, W. Mai, Y. Gu, Y. Gao, C. T. Huang, Y. Liu, L. J. Chen, Z. L. Wang, *Adv. Mater.* **2008**, *20*, 3919.
[19] Y. Zhu, F. Xu, Q. Qin, W. Y. Fung, W. Lu, *Nano Lett.* **2009**, *9*, 3934.
[20] Since these contact-based methods cannot perfectly avoid the contact-induced experimental artifacts, sometimes noncontact methods, including an electric-field-induced resonance method, are preferred. However, such a noncontact method can estimate only elastic properties and cannot provide information about non-elastic behavior (yielding and plasticity).
[21] S. Q. Shu, Y. Yang, T. Fu, C. S. Wen, J. Lu, *J. Mater. Res.* **2009**, *24*, 1054.
[22] N. K. Chang, Y. S. Lin, C. Y. Chen, S. H. Chang, *Thin Solid Films* **2009**, *517*, 3695.
[23] W. Liu, K. Bonin, M. Guthold, *Rev. Sci. Instrum.* **2007**, *78*, 063707.
[24] From the viewpoint of a local bond average (LBA) approach for defect-free crystalline materials, one may argue that the equational origin for the elastic modulus E and yield strength σ_y should be different from each other because they are physically independent; E and σ_y are for an equilibrium and a non-equilibrium state, respectively. However, with a simple continuum mechanics viewpoint, E and σ_y can have the same mechanical origin (that is elastic stress-strain relationship), as σ_y should satisfy the constitutive equations for both elastic and plastic regimes. Also, it is noteworthy that, for estimating real σ_y, one should take into consideration the structural defects (whether crystalline defects or mechanical flaws) that practically control the yielding, plasticity, and failure of crystalline materials.
[25] W. D. Callister, *Fundamentals of Materials Science and Engineering: An Integrated Approach*, John Wiley & Sons, New York **2005**.
[26] B. Lawn, *Fracture of Brittle Solids*, Cambridge University Press, Cambridge, UK **1993**.
[27] G. M. Pharr, *Mater. Sci. Eng., A* **1998**, *253*, 151.
[28] B. Bhushan, X. Li, *Int. Mater. Rev.* **2003**, *48*, 125.
[29] Y. G. Jung, A. Pajares, R. Banerjee, B. R. Lawn, *Acta Mater.* **2004**, *52*, 3459.
[30] M. Hebbache, *Solid State Commun.* **2000**, *113*, 427.
[31] R. Hull, *Properties of Crystalline Silicon*, INSPEC, London, UK **1997**.
[32] W. C. Oliver, G. M. Pharr, *J. Mater. Res.* **1992**, *7*, 1564.
[33] K. L. Johnson, *Contact Mechanics*, Cambridge University Press, Cambridge, UK, **1985**.
[34] A. C. Fischer-Cripps, *J. Mater. Res.* **2007**, *22*, 3075.
[35] J. Lian, J. Wang, J. Y. Kim, J. Greer, *J. Mech. Phys. Solids* **2009**, *57*, 812.
[36] A. Heidelberg, L. T. Ngo, B. Wu, M. A. Phillips, S. Sharma, T. I. Kamins, J. E. Sader, J. J. Boland, *Nano Lett.* **2006**, *6*, 1101.
[37] C. Q. Sun, *Prog. Mater Sci.* **2009**, *54*, 179.
[38] X. J. Liu, J. W. Li, Z. F. Zhou, L. W. Yang, Z. S. Ma, G. F. Xie, Y. Pan, C. Q. Sun, *Appl. Phys. Lett.* **2009**, *94*, 131902.
[39] C. Battaglia, K. Gaal-Nagy, C. Monney, C. Didiot, E. F. Schwier, M. G. Garnier, G. Onida, P. Aebi, *J. Phys.: Condens. Matter* **2009**, *21*, 013001.
[40] H. Ni, X. Li, H. Gao, *Appl. Phys. Lett.* **2006**, *88*, 043108.
[41] B. Lee, R. E. Rudd, *Phys. Rev. B* **2007**, *75*, 195328.
[42] K. Kang, W. Cai, *Int. J. Plast.* **2010**, *26*, 1387..
[43] G. Yu, J. Watanabe, K. Izumi, K. Nakashima, *Jpn. J. Appl. Phys,* **2001**, *40,* L183.
[44] P. M. Nagy, D. Aranyi, P. Horvath, G. Peto, E. Kalman, *Surf. Interface Anal.* **2008**, *40*, 875.
[45] B. Bhushan, X. Li, *J. Mater. Res.* **1997**, *12*, 54.
[46] Z. Zeng, X. Ma. J. Chen, Y. Zeng, D. Yang, Y. Liu, *J. Appl. Phys.* **2010**, *107*, 123503.
[47] K.-S. Son, D. H. Lee, J.-W. Choung, Y. B. Pyun, W. I. Park, T. Song, U. Paik, *J. Mater. Res.* **2008**, *23*, 3403.
[48] A. Javey, S. W. Nam, R. S. Friedman, H. Yan, C. M. Lieber, *Nano Lett.* **2007**, *7*, 773.